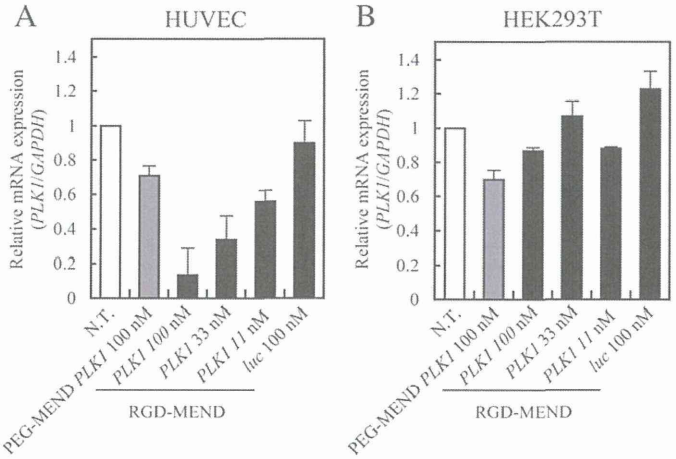

Fig. 3. Gene silencing effect of PEG-MEND and RGD-MEND. Cells were seeded on a 6-well plate 24 h prior to the MEND treatment, and the MENDs were then added to cells at the indicated concentrations for 24 h. Target gene mRNA expression was determined by qRT-PCR 24 h after the addition of PEG-MEND and RGD-MEND. *PLK1* expression was normalized to *GAPDH*.

of tumor wet tissue on day 17 compared to si-*luc* (Fig. 6B, C). To investigate whether *Vegfr2* suppression led to the inhibition of angiogenesis, vessels in tumor tissue were observed after 2 si-*Vegfr2* injections of 3.0 mg/kg by CLSM (Fig. 6D) The anti-angiogenesis effect was then evaluated by counting pixels indicating vessels; the vessels were significantly decreased in the si-*Vegfr2* group (Fig. 6E).

To evaluate the toxicity of systemically injected 3.0 mg/kg of RGD-MEND, we monitored changes in body weight during the treatment and also measured liver toxicity. No body weight change was observed in the OS-RC-2-bearing mice (Fig. 7A). Moreover, liposomal carriers sometimes severely injure the liver as liposomes tend to accumulate in liver. The activity of liver enzymes, AST and ALT, were not increased in the ICR mice at 24 h after the injection of 3.0 mg/kg MENDs (Fig. 7B).

4. Discussion

The cRGD peptide is a well-known ligand for both cancer cells and TECs. Although cRGD has been widely used as a targeting ligand for oligonucleotide delivery to TECs, there are few reports directly showing TEC-specific gene silencing mediated by siRNA. In this study, we verified that the RGD-MEND is capable of inducing siRNA-mediated gene silencing in TECs and attempted to develop a cancer therapy through an anti-angiogenic effect by delivering siRNA.

As previously described, the apparent pKa of the carrier is a dominant factor for escaping from endosomes in pH responsive carriers [10]. After internalization via endocytosis, the YSK-MEND is rapidly converted into a cationic molecule in response to acidification in the endosomes, and, consequently, the endosomal membrane is disrupted by interacting with endosomal membranes with a negative charge. Therefore, it is important to adjust the pKa of the particle to around 6.5 in order to rapidly respond the declining pH in endosomes. The apparent pKa of the RGD-MEND was compared with the RGD-modified MEND. As a result, the pKa was around 6.5 and remained unchanged as the result of the modification of RGD (Fig S2). This suggests that the RGD-MEND would be able to efficiently escape from the endosome in response to endosome acidification after internalization mediated by $\alpha_V\beta_3$ integrin–RGD interaction. Five mole percent (mol%) of RGD-modification resulted in the maximum cellular uptake in HUVEC cells, whereas additional RGD-modification had no further effect on uptake. This saturation might be due to fixed quantity of $\alpha_V\beta_3$ integrin present on HUVEC cells. In addition, it was previously reported that the PEGylation ratio in liposomes was, at most, 5.0 mol% [35]. Collectively, 5.0 mol% of RGD-PEG might be the optimized modification condition in both aspects of cells and siRNA carriers.

Table 2
Characteristics of the YSK-MENDs used in the in vivo experiments.

	RGD-MEND	PEG-MEND	conventional YSK-MEND
Lipid composition	YSK05/POPE/chol/PEG-DMG/RGD-PEG 50/25/25/3/5	YSK05/POPE/chol/PEG-DMG/PEG-DSPE 50/25/25/3/5	YSK05/DSPC/chol PEG-DSG 50/10/40/3
Diameter (nm)	115 ± 10	115 ± 17	105 ± 10
PdI	0.18 ± 0.01	0.21 ± 0.03	0.16 ± 0.04
ζ-potential (mV)	−18 ± 4	−18 ± 14	2.8 ± 1.4

The above mentioned properties on internalization via $\alpha_V\beta_3$ integrin and pH responsive fusiogenicity allows RGD-MEND to achieve a significant level of gene silencing in TECs at a dose of si-*Cd31* 4.0 mg/kg (Fig. 5). Nevertheless, gene silencing was saturated at 50% of N.T. In addition, two injections of 4.0 mg/kg of the RGD-MEND failed to drastically improve gene silencing (data not shown). This saturation might be caused by a limited distribution of the RGD-MEND in tumor tissue. When the distribution in tumor tissue was measured after systemic injection of the RGD-MEND, the fluorescence derived from the RGD-MEND was detected in approximately 80% of the TECs (Fig. S5). As the tumor vasculature is more heterogenous than normal tissue, blood flow is not sufficient in some parts of tumor vessels [36,37]. This heterogeneity in blood flow could lead to a limited distribution of the systemically delivered RGD-MEND.

As gene silencing in endothelial cells in normal organs would cause undesirable adverse effects, we determined the extent of accumulation in plasma, liver, spleen, kidney and lung by the RI-labeled not-PEGylated YSK-MEND (MEND), the PEG-MEND and the RGD-MEND containing RIs were injected into ICR mice, and the radio activity of these tissues were then measured (Fig. S7). Only the PEG-MEND showed a prolonged circulation time, while the others did not. Notably, a significant increased accumulation of RGD-MEND was observed in the spleen and lungs. The MEND accumulated most highly in the liver of three MENDs. The increased accumulation in the spleen can be attributed to platelets, which are abundant in the spleen. Platelets express $\alpha_{IIb}\beta_3$ integrin, which has a relatively similar structure to $\alpha_V\beta_3$ integrin [38]. As cRGD can also weakly bind to the $\alpha_{IIb}\beta_3$ integrin, the RGD-MEND may have accumulated in spleen. Though the mechanism responsible for the high accumulation of RGD-MEND in lungs is currently unclear, the cRGD conjugated oligopeptide–plasmid DNA complex also

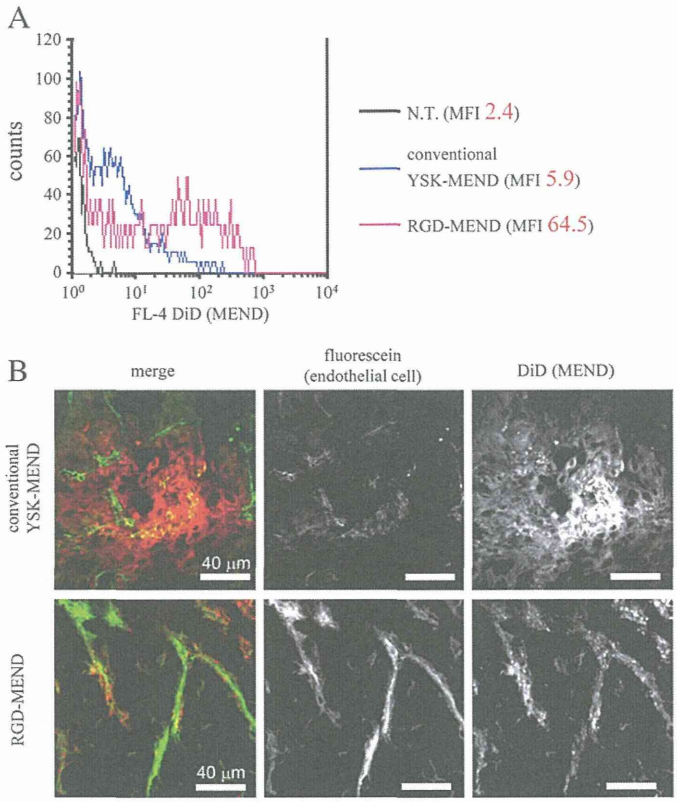

Fig. 4. Analysis of the localization of RGD-MEND in tumor tissue. Mean of the fluorescence intensity (MFI) of DiD in the CD31 positive population of tumor burden was compared among MENDs. B) DiD-labeled MENDs were injected into OS-RC-2-bearing mice, and 6 h after the injection, tumor tissues were collected and observed by CLSM. In merged images, green and red dots mean endothelial cells and MENDs, respectively. Upper panels show the images of conventional YSK-MEND and lower shows the images of RGD-MEND. Scale bars are 40 μm. N.T.: non treatment.

accumulated at slightly higher levels in the lungs compared to the un-modified version used in a previous report [39]. Thus, a modest higher accumulation in the lungs must be accompanied by cRGD modification. Taking into consideration the fact that the highest accumulation was in the liver and an increased accumulation was found in the lungs and spleen, *Cd31* gene silencing in these organs were evaluated 24 h after injection of the RGD-MEND. No significant gene reduction was observed in any of these organs (Fig. S9). Although a modestly higher accumulation of the RGD-MEND in the spleen and lungs was observed, there is little possibility that the systemic injection of RGD-MEND induced side effects in other organs. In the case of present anti-angiogenic agents, the inhibitory effect on angiogenesis in normal tissue, except for tumor tissue, can lead to an unfavorable influence. For example, Avastin can induce mortal side effects, such as bowel perforation and pulmonary hemorrhages because Avastin can inhibit VEGF signaling in normal tissue, which is required for the maintenance of healthy blood

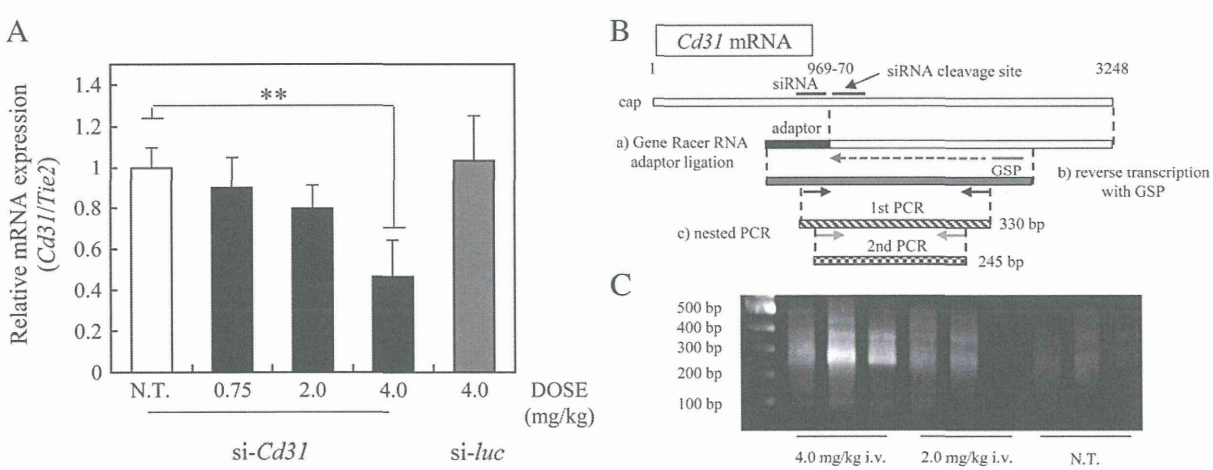

Fig. 5. Gene silencing via RNAi after injection of RGD-MEND. A) siRNA formulated in RGD-MEND was injected into OS-RC-2-bearing mice were injected at the indicated doses, and 24 h after the injection, *Cd31* expression was determined by qRT-PCR. B) Schematic diagram of the 5′ RACE-PCR method. Predicted cleavage site by si-*Cd31* was *Cd31* mRNA (3248 bp) and is indicated by an arrow between 969 and 970 bp of *Cd31 mRNA*. siRNA specific cleavage was detected as follows. First, the Gene Racer RNA adaptor was ligated into cleaved uncapped *Cd31* mRNA, and adaptor-ligated mRNA was then reverse transcribed with the gene specific primer (GSP). Next, complementary DNA was amplified by PCR with two independent primer sets (nested PCR). As a result, the production of 245 bp PCR fragment is indicative of siRNA-specific cleavage. C) The actual gel image of the 5′ RACE-PCR products. RNA extracted from tumor-bearing mice which were treated with 4.0 or 2.0 mg/kg siRNA encapsulated in RGD-MEND was subjected to a 5′ RACE-PCR procedure. N.T.: non treatment.

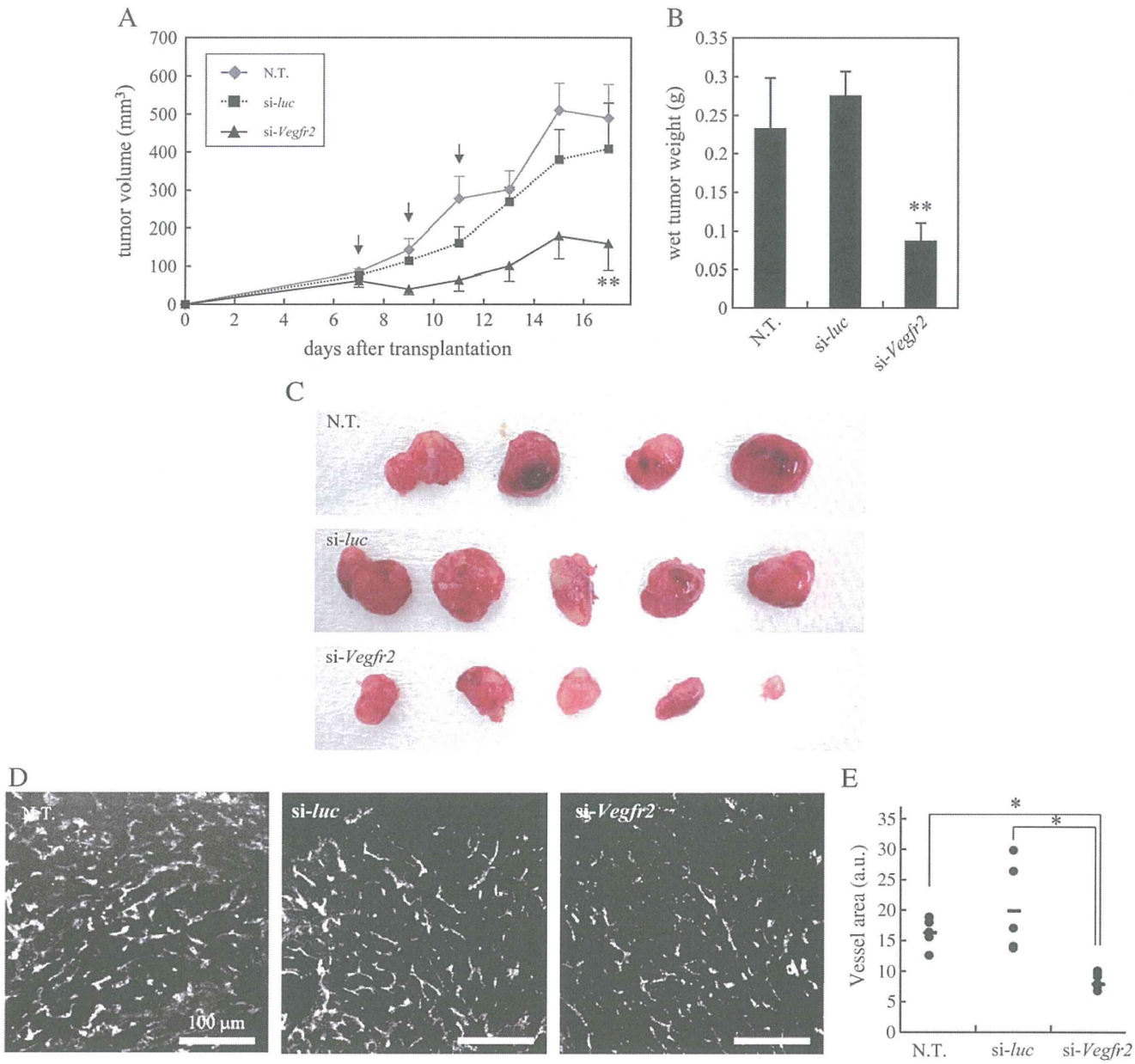

Fig. 6. Anti-tumor effect of si-*Vegfr2* encapsulated in RGD-MEND. A) RGD-MENDs encapsulating si-*luc* or si-*Vegfr2* were injected 3 times on alternate days at a dose of 3.0 mg/kg. Tumor volume was chronologically measured until day 17. Arrows denote the injection of the MEND. B) Wet tumor tissue was weighed when tumor was excised 17 days after transplantation. C) Photographs of collected tumor tissues. **: $p < 0.05$ (ANOVA followed by Bonferroni correction vs. N.T., $n = 5$). D) A typical image of each group is shown. Tumor bearing mice were injected with MENDs into tail vein twice. Twenty four hours after the injection, tumor tissues were excised and observed with CLSM. Scale bars are 100 μm. E) Pixels showing vessels, which were stained by isolectin B4, were counted with ImageJ. *; $p < 0.05$: ANOVA followed by SNK test, $n = 5–7$. N.T.: non treatment.

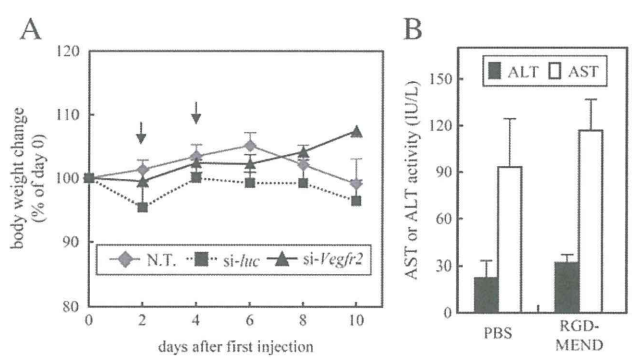

Fig. 7. Somatic and liver toxicological analyses of the RGD-MEND. A) The change in body weight was monitored after the first therapeutic injections into nude mice at a dose of 3.0 mg/kg every other day. Arrows show MENDs injection. B) Liver toxicity was evaluated by measuring the activities of selected liver enzymes, namely, ALT (black column) and AST (white column). These assays were performed 24 h after the injection of the RGD-MEND at a dose of 3.0 mg/kg. $n = 3$. N.T.: non treatment.

vessels [40,41]. In contrast, since the RGD-MEND could selectively suppress gene expression in tumor tissue, its use should be safer than the currently used anti-angiogenic agents.

Although OS-RC-2 cells were $\alpha_V\beta_3$ integrin positive (data not shown), no significant knockdown was observed in cancer cells (Fig. S8). The failure of cancer cell gene silencing was probably due to the lack of spreading of RGD-MEND in tumor tissue. Actually, almost all of the RGD-MEND appeared to remain in tumor vessels in the CLSM result (Fig. 5B). Although long-circulating liposomes can accumulate in tumor tissue after intravenous administration via the EPR effect as described above, the RGD-MEND failed to accumulate and diffuse in tumor tissue because of the instability of the RGD-MEND in the bloodstream (Fig. S7).

Although some groups reported on the therapeutic effect of cRGD itself, the injection of RGD-MEND encapsulating si-*luc* failed to inhibit tumor growth (Fig. 6A). In the reports dealing with the therapeutic effects of cRGD, the dosage of cRGD was 10–30 mg/kg [19,42,43]. On the other hand, the amount of cRGD was 1.6 mg/kg in the case of 4.0 mg/kg of cRGD-MEND. These facts suggest that the amount of cRGD on the RGD-MEND was insufficient to produce a curative effect. In contrast, tumor growth in the group treated with si-*Vegfr2* was markedly delayed. To exclude the possibility that si-*Vegfr2* led to cell death in OS-RC-2 cells themselves, we examined the effect of si-*Vegfr2* transfection to OS-RC-2 cells on viability. When OS-RC-2 cells were treated with si-*Vegfr2* and si-*luc*, no detectable reduction in cell viability compared to N.T. was found in both groups (Fig. S11). These results suggest that the injection of si-*Vegfr2* inhibits tumor growth via angiogenic gene knockdown in TECs.

5. Conclusions

The RGD-MEND caused significant gene silencing in tumor endothelial cells, but not in endothelial cells in normal organs and cancer cells without severe toxicity. In addition, 5′ RACE-PCR revealed that siRNA-mediated RNA interference was responsible for the gene reduction observed in TECs. In other words, we succeeded in developing an efficient system for the delivery of siRNA specifically to tumor endothelial cells. This system is a promising siRNA delivery system for investigations of the pathological characteristics of tumor endothelial cells, and moreover for cancer treatment via controlling of the biological function of tumor endothelial cells.

Grant support

This study was supported in part by a Grant-in-Aid for Research Activity Start-up (Grant Number 25893001), a Grant-in-Aid for Scientific Research on Innovative Areas "Nanomedicine Molecular Science" (No. 2306) from Ministry of Education, Culture, Sports, Science, and Technology (MEXT) of Japan, and the Special Education and Research Expenses of the Ministry of Education, Culture, Sports, Science and Technology (MEXT) of Japan.

Acknowledgments

The authors also wish to thank Dr. Milton S. Feather for his helpful advice in writing the English manuscript.

Appendix A. Supplementary data

Supplementary data to this article can be found online at http://dx.doi.org/10.1016/j.jconrel.2013.10.003.

References

[1] N. Ferrara, R.S. Kerbel, Angiogenesis as a therapeutic target, Nature 438 (2005) 967–974.
[2] L.M. Ellis, D.J. Hicklin, VEGF-targeted therapy: mechanisms of anti-tumour activity, Nat. Rev. Cancer 8 (2008) 579–591.
[3] J. Folkman, Tumor angiogenesis: therapeutic implications, N. Engl. J. Med. 285 (1971) 1182–1186.
[4] C. Harrison, Angiogenesis: a deeper understanding of VEGFR inhibitors, Nat. Rev. Cancer 12 (2012) 735.
[5] C. Harrison, Anticancer drugs: a deeper understanding of VEGFR inhibitors, Nat. Rev. Drug Discov. 11 (2012) 831.
[6] K.A. Whitehead, R. Langer, D.G. Anderson, Knocking down barriers: advances in siRNA delivery, Nat. Rev. Drug Discov. 8 (2009) 129–138.
[7] G.R. Rettig, M.A. Behlke, Progress toward *in vivo* use of siRNAs-II, Mol. Ther. 20 (2012) 483–512.
[8] K. Kogure, H. Akita, Y. Yamada, H. Harashima, Multifunctional envelope-type nano device (MEND) as a non-viral gene delivery system, Adv. Drug Deliv. Rev. 60 (2008) 559–571.
[9] H. Hatakeyama, H. Akita, H. Harashima, A multifunctional envelope type nano device (MEND) for gene delivery to tumours based on the EPR effect: a strategy for overcoming the PEG dilemma, Adv. Drug Deliv. Rev. 63 (2011) 152–160.
[10] Y. Sato, H. Hatakeyama, Y. Sakurai, M. Hyodo, H. Akita, H. Harashima, A pH-sensitive cationic lipid facilitates the delivery of liposomal siRNA and gene silencing activity *in vitro* and *in vivo*, J. Control. Release 163 (2012) 267–276.
[11] Y. Sakurai, H. Hatakeyama, Y. Sato, M. Hyodo, H. Akita, H. Harashima, Gene silencing via RNAi and siRNA quantification in tumor tissue using MEND, a liposomal siRNA delivery system, Mol. Ther. 2 (2013) 1195–1203.
[12] A.D. Judge, M. Robbins, I. Tavakoli, J. Levi, L. Hu, A. Fronda, E. Ambegia, K. McClintock, I. MacLachlan, Confirming the RNAi-mediated mechanism of action of siRNA-based cancer therapeutics in mice, J. Clin. Invest. 119 (2009) 661–673.
[13] S.C. Semple, A. Akinc, J. Chen, A.P. Sandhu, B.L. Mui, C.K. Cho, D.W. Sah, D. Stebbing, E.J. Crosley, E. Yaworski, I.M. Hafez, J.R. Dorkin, J. Qin, K. Lam, K.G. Rajeev, K.F. Wong, L.B. Jeffs, L. Nechev, M.L. Eisenhardt, M. Jayaraman, M. Kazem, M.A. Maier, M. Srinivasulu, M.J. Weinstein, Q. Chen, R. Alvarez, S.A. Barros, S. De, S.K. Klimuk, T. Borland, V. Kosovrasti, W.L. Cantley, Y.K. Tam, M. Manoharan, M.A. Ciufolini, M.A. Tracy, A. de Fougerolles, I. MacLachlan, P.R. Cullis, T.D. Madden, M.J. Hope, Rational design of cationic lipids for siRNA delivery, Nat. Biotechnol. 28 (2010) 172–176.
[14] M. Meyer, A. Philipp, R. Oskuee, C. Schmidt, E. Wagner, Breathing life into polycations: functionalization with pH-responsive endosomolytic peptides and polyethylene glycol enables siRNA delivery, J. Am. Chem. Soc. 130 (2008) 3272–3273.
[15] H. Yu, Y. Zou, Y. Wang, X. Huang, G. Huang, B.D. Sumer, D.A. Boothman, J. Gao, Overcoming endosomal barrier by amphotericin B-loaded dual pH-responsive PDMA-b-PDPA micelleplexes for siRNA delivery, ACS Nano 5 (2011) 9246–9255.
[16] V.P. Torchilin, Recent advances with liposomes as pharmaceutical carriers, Nat. Rev. Drug Discov. 4 (2005) 145–160.
[17] C.J. Avraamides, B. Garmy-Susini, J.A. Varner, Integrins in angiogenesis and lymphangiogenesis, Nat. Rev. Cancer 8 (2008) 604–617.
[18] C. Mas-Moruno, F. Rechenmacher, H. Kessler, Cilengitide: the first anti-angiogenic small molecule drug candidate design, synthesis and clinical evaluation, Anticancer Agents Med. Chem. 10 (2010) 753–768.
[19] P.C. Brooks, A.M. Montgomery, M. Rosenfeld, R.A. Reisfeld, T. Hu, G. Klier, D.A. Cheresh, Integrin alpha v beta 3 antagonists promote tumor regression by inducing apoptosis of angiogenic blood vessels, Cell 79 (1994) 1157–1164.
[20] F. Danhier, A. Le Breton, V. Preat, RGD-based strategies to target alpha(v) beta(3) integrin in cancer therapy and diagnosis, Mol. Pharm. 9 (2012) 2961–2973.
[21] R.J. Christie, Y. Matsumoto, K. Miyata, T. Nomoto, S. Fukushima, K. Osada, J. Halnaut, F. Pittella, H.J. Kim, N. Nishiyama, K. Kataoka, Targeted polymeric micelles for siRNA treatment of experimental cancer by intravenous injection, ACS Nano 6 (2012) 5174–5189.
[22] E. Kenjo, T. Asai, N. Yonenaga, H. Ando, T. Ishii, K. Hatanaka, K. Shimizu, Y. Urita, T. Dewa, M. Nango, H. Tsukada, N. Oku, Systemic delivery of small interfering RNA by use of targeted polycation liposomes for cancer therapy, Biol. Pharm. Bull. 36 (2013) 287–291.
[23] T. Tagami, T. Suzuki, M. Matsunaga, K. Nakamura, N. Moriyoshi, T. Ishida, H. Kiwada, Anti-angiogenic therapy via cationic liposome-mediated systemic siRNA delivery, Int. J. Pharm. 422 (2012) 280–289.
[24] S. Anand, B.K. Majeti, L.M. Acevedo, E.A. Murphy, R. Mukthavaram, L. Scheppke, M. Huang, D.J. Shields, J.N. Lindquist, P.E. Lapinski, P.D. King, S.M. Weis, D.A. Cheresh, MicroRNA-132-mediated loss of p120RasGAP activates the endothelium to facilitate pathological angiogenesis, Nat. Med. 16 (2010) 909–914.
[25] D.Y. Heng, R.M. Bukowski, Anti-angiogenic targets in the treatment of advanced renal cell carcinoma, Curr. Cancer Drug Targets 8 (2008) 676–682.
[26] B. Escudier, Emerging immunotherapies for renal cell carcinoma, Ann. Oncol. 23 (Suppl. 8) (2012) viii35–viii40.
[27] G. Bergers, D. Hanahan, Modes of resistance to anti-angiogenic therapy, Nat. Rev. Cancer 8 (2008) 592–603.
[28] J.S. Ko, P. Rayman, J. Ireland, S. Swaidani, G. Li, K.D. Bunting, B. Rini, J.H. Finke, P.A. Cohen, Direct and differential suppression of myeloid-derived suppressor cell subsets by sunitinib is compartmentally constrained, Cancer Res. 70 (2010) 3526–3536.
[29] I. Helfrich, I. Scheffrahn, S. Bartling, J. Weis, V. von Felbert, M. Middleton, M. Kato, S. Ergun, D. Schadendorf, Resistance to antiangiogenic therapy is directed by vascular phenotype, vessel stabilization, and maturation in malignant melanoma, J. Exp. Med. 207 (2010) 491–503.
[30] G. Kibria, H. Hatakeyama, N. Ohga, K. Hida, H. Harashima, Dual-ligand modification of PEGylated liposomes shows better cell selectivity and efficient gene delivery, J. Control. Release 153 (2011) 141–148.
[31] N. Ohga, K. Hida, Y. Hida, C. Muraki, K. Tsuchiya, K. Matsuda, Y. Ohiro, Y. Totsuka, M. Shindoh, Inhibitory effects of epigallocatechin-3 gallate, a polyphenol in green tea, on tumor-associated endothelial cells and endothelial progenitor cells, Cancer Sci. 100 (2009) 1963–1970.

[32] H. Maeda, Y. Matsumura, H. Kato, Purification and identification of [hydroxyprolyl3] bradykinin in ascitic fluid from a patient with gastric cancer, J. Biol. Chem. 263 (1988) 16051–16054.
[33] R.A. Brekken, J.P. Overholser, V.A. Stastny, J. Waltenberger, J.D. Minna, P.E. Thorpe, Selective inhibition of vascular endothelial growth factor (VEGF) receptor 2 (KDR/Flk-1) activity by a monoclonal anti-VEGF antibody blocks tumor growth in mice, Cancer Res. 60 (2000) 5117–5124.
[34] I.J. Duignan, E. Corcoran, A. Pennello, M.J. Plym, M. Amatulli, N. Claros, M. Iacolina, H. Youssoufian, L. Witte, S. Samakoglu, J. Schwartz, D. Surguladze, J.R. Tonra, Pleiotropic stromal effects of vascular endothelial growth factor receptor 2 antibody therapy in renal cell carcinoma models, Neoplasia 13 (2011) 49–59.
[35] K. Sou, T. Endo, S. Takeoka, E. Tsuchida, Poly(ethylene glycol)-modification of the phospholipid vesicles by using the spontaneous incorporation of poly(ethylene glycol)-lipid into the vesicles, Bioconjug. Chem. 11 (2000) 372–379.
[36] P. Vaupel, F. Kallinowski, P. Okunieff, Blood flow, oxygen and nutrient supply, and metabolic microenvironment of human tumors: a review, Cancer Res. 49 (1989) 6449–6465.
[37] A.R. Pries, A.J. Cornelissen, A.A. Sloot, M. Hinkeldey, M.R. Dreher, M. Hopfner, M.W. Dewhirst, T.W. Secomb, Structural adaptation and heterogeneity of normal and tumor microvascular networks, PLoS Comput. Biol. 5 (2009) e1000394.
[38] F. Bianchini, N. Cini, A. Trabocchi, A. Bottoncetti, S. Raspanti, E. Vanzi, G. Menchi, A. Guarna, A. Pupi, L. Calorini, (1)(2)(5)I-radiolabeled morpholine-containing arginine-glycine-aspartate (RGD) ligand of alphavbeta(3) integrin as a molecular imaging probe for angiogenesis, J. Med. Chem. 55 (2012) 5024–5033.
[39] Y. Aoki, S. Hosaka, S. Kawa, K. Kiyosawa, Potential tumor-targeting peptide vector of histidylated oligolysine conjugated to a tumor-homing RGD motif, Cancer Gene Ther. 8 (2001) 783–787.
[40] T. Eisen, C.N. Sternberg, C. Robert, P. Mulders, L. Pyle, S. Zbinden, H. Izzedine, B. Escudier, Targeted therapies for renal cell carcinoma: review of adverse event management strategies, J. Natl. Cancer Inst. 104 (2012) 93–113.
[41] S. Goel, D.G. Duda, L. Xu, L.L. Munn, Y. Boucher, D. Fukumura, R.K. Jain, Normalization of the vasculature for treatment of cancer and other diseases, Physiol. Rev. 91 (2011) 1071–1121.
[42] F. Mitjans, T. Meyer, C. Fittschen, S. Goodman, A. Jonczyk, J.F. Marshall, G. Reyes, J. Piulats, *In vivo* therapy of malignant melanoma by means of antagonists of alphav integrins, Int. J. Cancer 87 (2000) 716–723.
[43] M.A. Buerkle, S.A. Pahernik, A. Sutter, A. Jonczyk, K. Messmer, M. Dellian, Inhibition of the alpha-nu integrins with a cyclic RGD peptide impairs angiogenesis, growth and metastasis of solid tumours *in vivo*, Br. J. Cancer 86 (2002) 788–795.

International Journal of Pharmaceutics 456 (2013) 195–201

Contents lists available at ScienceDirect

International Journal of Pharmaceutics

journal homepage: www.elsevier.com/locate/ijpharm

Pharmaceutical nanotechnology

A liposomal delivery system that targets liver endothelial cells based on a new peptide motif present in the ApoB-100 sequence

Afsana Akhter[a,c], Yasuhiro Hayashi[a,c], Yu Sakurai[a,c], Noritaka Ohga[b,c], Kyoko Hida[b,c], Hideyoshi Harashima[a,b,c,*]

[a] Laboratory of Innovative Nanomedicine, Faculty of Pharmaceutical Sciences, Hokkaido University, Kita 12, Nishi 6, Kita-ku, Sapporo 060-0812, Japan
[b] Laboratory for Molecular Design of Pharmaceutics, Faculty of Pharmaceutical Sciences, Hokkaido University, Kita-12, Nishi-6, Kita-ku, Sapporo, Hokkaido 060-0812, Japan
[c] Division of Vascular Biology, Graduate School of Dental Medicine, Hokkaido University, Kita 13 Nishi 7, Kita-ku, Sapporo 060-0812, Japan

ARTICLE INFO

Article history:
Available online 7 August 2013

Keywords:
ApoB-100 sequence
CSPG
LDL receptor
Liver endothelial cell
RLTR peptide
KLGR peptide

ABSTRACT

Liver dysfunction is associated with a variety of liver diseases, including viral or alcoholic hepatitis, fibrosis, cirrhosis, and portal hypertension. A targeted drug delivery system would be very useful in the treatment of these diseases. We herein describe the development of a system comprised of a new peptide–lipid conjugate for the efficient delivery of molecules to LEC. The RLTRKRGLK sequence (3359–3367), which mediates the association of LDL with arterial CSPG and an LDL receptor, was utilized as a ligand for achieving this goal. The peptide modified PEG-LPs (RLTR-PEG-LPs) were efficiently taken up by primary liver endothelial cells (liver ECs) and other types of cells. In vivo biodistribution and confocal microscopy analysis showed that RLTR-PEG-LPs became widely accumulated in LECs within a short time. Distribution of RLTR-PEG-LPs was greatly reduced with a pretreatment of unlabeled RLTR-PEG-LPs, not cationic LPs, indicating that the sequence is important for LECs. The findings indicate that a reverse sequence of RLTR (KLGR) modified PEG-LPs (KLGR-PEG-LP) did the same pattern compared with RLTR-PEG-LPs, suggesting that the RKR or RXXR sequence might be essential for LECs targeting. Collectively RLTR-PEG-LPs and KLGR-PEG-LPs have the potential for delivering drugs to LECs.

1. Introduction

The liver is the largest organ of the body and is probably the most important power and sewage treatment plant in the body. Two major types of cells populate the liver, namely, parenchymal and non-parenchymal cells. Approximately 80% of the liver volume is made up of parenchymal cells commonly referred to as hepatocytes (Ramadori et al., 2008). Sinusoidal endothelial cells, Kupffer cells and hepatic stellate cells are examples of non-parenchymal cells. Different types of liver diseases are associated with different types of liver cells. For example viral hepatitis and alcoholic hepatitis are associated with hepatocytes. Liver endothelial cell (LEC) dysfunction is associated with variety of liver diseases, including fibrosis, cirrhosis, and portal hypertension (Dominique and Vijay, 2010). The defenestration of liver endothelial cells causes hyperlipidemia, because it becomes difficult for lipoproteins to reach hepatocytes (Rajkumar et al., 2010). Kupffer cells are associated with the progression of non-alcoholic steatosis and fibrosis. It has also been reported that hepatocellular stress caused by various diseases causes the release of different types of cytokines and chemokines by different types of cells which ultimately cause the transmigration of inflammatory cells toward their target, hepatocytes (Ramadori et al., 2008). Therefore, a selective drug delivery system would be an ideal approach for achieving a subsequent efficient therapy for treating different types of liver diseases.

A group of certain basic proteins or peptides have the ability to inhibit the binding of low density lipoprotein (LDL) to its receptor protein (Brown et al., 1978). This inhibition is caused by polycations interacting with the receptor. LDLs are associated with a negatively charged LDL receptor even though the net charge of this lipoprotein is also negative. This suggests that the net charge of the LDL is governed by the positive charge of the ApoB sequence. Two basic regions of similar size in ApoB-100 segments, namely 3147 through 3157 and 3359 through 3367 are part of the LDL receptor binding domain. This ApoB heterodimer binds to the LDL receptor and also binds with Glycoseaminoglycans (GAGs) with an affinity similar to that between LDL and GAGs (Urban et al., 1997). The ApoB-100 segment RLTRKRGLK (3359–3367) is a mediator of the association between LDL and arterial Chondroitin sulfate-rich proteoglycan

* Corresponding author at: Faculty of Pharmaceutical Sciences, Hokkaido University, Kita-12, Nishi-6, Kita-ku, Sapporo, Hokkaido 060-0812, Japan.
Tel.: +81 11 706 3919; fax: +81 11 706 4879.
E-mail address: harasima@pharm.hokudai.ac.jp (H. Harashima).

0378-5173/$ – see front matter © 2013 Elsevier B.V. All rights reserved.
http://dx.doi.org/10.1016/j.ijpharm.2013.07.068

(CSPG) (Urban et al., 1993). It has recently been reported that LEC express low density lipoprotein receptor protein-1 (LRP-1) which is a member of the LDL receptor gene family (Oie et al., 2011; Thomas et al., 1999). Another study has shown that LDL is taken up by both parenchymal and non-parenchymal cells (Marit et al., 1998).

Liposomes are suitable nano-carriers that have the capacity to deliver drug particles to various target cells in vitro or diseased tissues in vivo (Puri et al., 2009; Du et al., 2007). Based on these considerations, we selected the ApoB segment RLTRKRGLK (3359–3367) abbreviated here as RLTR for use as a novel ligand in designing a selective targeting system for hepatocytes. Surprisingly, however, this carrier system was accumulated through the blood vessels in the liver. In order to examine the targeting ability of this RLTR modified liposome, our efforts were focused on two parameters, one being the cationic nature of this peptide and second the essential peptide sequence.

2. Materials and methods

2.1. Materials

Cholesterol (Chol), 1,2-dioleoyl-sn-glycero-3-phosphoethanolamine (DOPE), diethanolamine chloride (DC-6-14), Egg phosphatidylcholine (EPC), N-(lissamine rhodamine B sulfonyl) -1,2-dioleoyl-sn-glycero-3-phosphoethanolamine (rhodamine -DOPE), 1,2-distearoyl-*sn*-glycero-3-phosphoethanolamine-N-[methoxy (polyethyleneglycol)-2000] (PEG_{2000}-DSPE) were purchased from Avanti Polar Lipids (Alabaster, AL, USA). N-[(3-maleimide-1-oxopropyl) aminopropyl polyethyleneglycol-carbamyl] distearoylphosphatidyl-ethanolamine (maleimide-PEG-DSPE) was purchased from Nippon Oil and Fat Co. (Tokyo, Japan). ^{3}H-Cholesteryl hexadecyl ether (CHE) were purchased from New England Nuclear (USA). RLTRKRGLKGGC (RLTR in brief) and KLGRKRTLRGGC (KLGR in brief) peptides were purchased from Kurabo Industries, Osaka, Japan. Endothelial Cell Basal Medium (EBM-2) and other related growth factors were purchased from Lonza (Walkersville, MD, USA). Dulbecco's fetal bovine serum (FBS) was obtained from Hyclone Laboratories (Logan, UT, USA). All other chemicals used in this study were of analytical grade.

2.2. Animals

4–5 week old male ICR mice were purchased from Japan SLC (Shizuoka, Japan). The experimental protocols were reviewed and approved by the Hokkaido University Animal Care Committee in accordance with the guidelines for care and use of Laboratory animals. Animals were used without fasting in all experiments.

2.3. Conjugation of the RLTR peptide to PEG_{2000}-DSPE

Peptides conjugated with glycine–glycine–cysteine (GGC) sequence at the N-terminal were purchased from commercial sources. Actually the GGC linker was added to the N-terminal to facilitate the binding of the thiol group of cysteine residue to the pyrrole group of Maleimide-PEG_{2000}-DSPE. The additional Gly-Gly (GG) amino acid was added to increase the flexibility of the peptide ligand attached on the top of Mal-PEG_{2000}-DSPE. Conjugation was achieved by incubating a 1.2:1 molar ratio of RLTRKRGLKGGC peptide and maleimide-PEG-DSPE in deionized water at room temperature for 24 h. The conjugation of RLTR with PEG was confirmed by matrix assisted laser desorption/ionization-time of flight (MALDI-TOF) MS (Bruker Daltonics, Germany) using acetonitrile:water = 7:3 with 0.1% of trifluoroacetate as the matrix solution, supplied with a 10 mg/ml solution of dihydroxybenzoic acid.

2.4. Preparation of liposomes

Liposomes (LPs) composed of EPC/Chol (molar ratio: 7/3) was prepared by the lipid hydration method. A control cationic LP was prepared using DC6-14, DOPE, and Cholesterol at a molar ratio of 4:3:3 (Ishiwata et al., 2000). RLTR peptide modified PEG-LPs (RLTR-PEG-LPs) were prepared by adding the required amount of RLTR-PEG to the lipid solution. 1 mol% rhodamine-DOPE was incorporated, to serve as a label for the lipid component. A lipid film was produced by evaporation of the solvents (chloroform and ethanol) from a lipid solution in a glass tube. HEPES buffer (10 mM, pH 7.4) was added and the solution was incubated for 10 min to hydrate the lipid film. The glass tube was then sonicated for approximately 30 s in a bath-type sonicator (AU-25C, Aiwa, Tokyo, Japan). The mean size and zeta potential of the prepared LPs were determined using a Zetasizer Nano ZS ZEN3600 instrument (Malvern Instruments Ltd., Worchestershire, UK).

2.5. Isolation of primary liver endothelial cells (liver ECs)

Liver endothelial cells (liver ECs) were isolated as previously described (Hida et al., 2004; Akino et al., 2009; Ohga et al., 2009). Briefly, the liver of a female KSN mouse was excised. The excised tissue was minced and digested with collagenase II (Worthington, Freehold, NJ). Blood cells were removed by a single sucrose step-gradient centrifugation with Histopaque 1077 (Sigma-Aldrich), and the resulting cell suspension was filtered. Endothelial cells were isolated using MACS according to the manufacturer's instructions using a FITC-anti-CD31 antibody. CD31-positive cells were sorted and plated on 1.5% gelatin-coated culture plates and grown in EGM-2MV (Clonetics, Walkersville, MD) and 10% fetal bovine serum. After subculturing for 2 weeks, the isolated ECs were purified by a second round of purification using FITC-BS1-B4 (Vector Laboratories, Burlingame, CA). All of the endothelial cells were split at a ratio of 1:3.

2.6. In vitro cellular uptake study

For the cellular uptake study, 40,000 cells were seeded in a 24-well plate (Corning incorporated, Corning, NY, USA) (40,000 cells/well). After 24 h, the prepared rhodamine labeled PEG-LPs/RLTR-PEG-LPs were added and incubated for an additional 3 h. After the incubation, the cells were washed with PBS (pH 7.4) and then treated with Reporter Lysis Buffer (Promega Corp., Madison, WI, USA) followed by centrifugation at 12,000 rpm for 5 min at 4 °C to remove debris. The supernatants were then collected. The cellular uptake efficiency of the prepared rhodamine labeled LPs were determined by measuring the fluorescence intensity of rhodamine (excitation at 550 nm and emission at 590 nm) using FP-750 Spectrofluorometer (JAS Co., Tokyo, Japan).

2.7. In vivo biodistribution study

^{3}H-Cholesteryl hexadecyl ether (CHE) labeled LPs and RLTR-PEG-LPs were used to measure the biodistribution of liposomes in different organs in the mice. ICR mice were intravenously injected with ^{3}H-labeled LPs or RLTR-PEG-LPs. After 25 min, the animals were sacrificed; the portal vein was cut and a needle was introduced into the vena cava and 10–15 ml of heparin containing PBS (40 units/ml) solution was used to remove the remaining blood and cell surface bound RLTR-PEG-LPs in the liver. Other organs, including the lungs and kidney were also collected and all of the collected organs were weighed. After weighing, the samples were solubilized in Soluene-350 (Perkin-Elmer Life Sciences, Japan) for overnight at 55 °C. Samples were decolorized by treatment with H_2O_2. The radioactivity of the samples was

measured by using a liquid scintillation counting (LSC-6100, Aloka, Japan) after adding 10 ml of Hionic Flour (Perkin-Elmer Life Sciences, Japan) (Hatakeyama et al., 2004). Tissue accumulation of LPs was represented as the percentage of injected dose (%ID) per organ.

2.8. Confocal microscopy experiment

ICR mice were given intravenous injection of rhodamine labeled RLTR-PEG-LPs and the mice were killed 25 min after the treatment. The liver was perfused as mentioned in Section 2.7 and then it was collected. The liver was then excised and washed with saline and sliced into 10–15 mm-sized blocks with scissors. The liver sections were then incubated with a 20 fold volume of a diluted solution of Hoechst 33342 (1 mg/ml) and Isolectin B4 in HEPES buffer for 1 h. The specimens were placed on a 35 mm glass base dish (IWAKI, Osaka, Japan) and observed by confocal laser scanning microscopy (A1 Confocal Laser Microscope System, Nikon Instruments Inc., Tokyo, Japan).

2.9. Inhibition assay

2.9.1. In vivo competitive inhibition study of RLTR-PEG-LPs

ICR mice were injected with unlabeled LPs and after 15 min, they were injected with cationic LP or RLTR modified PEG-LP or KLGR (reverse peptide sequence of RLTR) modified PEG-LP. After another 25 min of incubation the mice were sacrificed and the livers were perfused with 10 ml of a 40% heparin-PBS solution. The mice livers were then collected, sliced into 0.5 mm × 0.5 mm pieces, stained with Hoechst 33342 and Isolectin B4 and then observed by confocal microscopy (A1 Confocal Laser Microscope System, Nikon Instruments Inc., Tokyo, Japan).

2.9.2. In vitro competitive inhibition study of RLTR-PEG-LPs

For in vitro inhibition study unlabeled RLTR-PEG or KLGR-PEG modified LPs were used as inhibitors. We previously used an excess amount of free RLTR or KLGR peptide as an inhibitor but no significant inhibition was observed (data not shown). It was reported that the monomeric free peptide might not be sufficiently effective to inhibit the interactions of multiplex RLTR-PEG-LP or KLGR-PEG-LP with the target receptor (Kibria et al., 2011). As a result we used unlabeled RLTR-PEG or KLGR-PEG modified LP as inhibitors in order to achieve multivalent attachment with the targeted receptors. Here 40,000 LECs were seeded in a 24-well plate and the plate was incubated overnight. After 24 h, different concentrations of rhodamine labeled and unlabeled PEG-LPs (1:0, 1:5, 1:10, 1:20 and 1:50 respectively) were added and incubated for 3 h. After 3 h, the cells were washed 3 times with 1 ml of ice-cold phosphate buffer saline (PBS) which was supplemented with heparin (20 units/ml) to completely remove the surface-bound RLTR-PEG-LP and the intracellular fluorescence intensity of rhodamine was then determined (Kibria et al., 2011).

Table 1
Physicochemical properties of the RLTR-PEG-LP.

% PEG	Properties			
	PEG-LP		RLTR-PEG-LP	
	Size (nm)	Z-potential (mV)	Size (nm)	Z-potential (mV)
0	92 ± 10	−5 ± 9	–	–
1	102 ± 8	−8 ± 5	115 ± 10	12 ± 4
3	100 ± 5	−20 ± 8	121 ± 14	20 ± 6
5	105 ± 7	−19 ± 11	135 ± 8	22 ± 8
10	110 ± 11	−24 ± 12	132 ± 10	27 ± 3

Data are presented as the mean ± SD ($n = 3$).

2.10. Statistical analysis

Comparisons between multiple treatments were made using one-way analysis of variance (ANOVA), followed by the 'Dunnett test'. Pair-wise comparisons of subgroups were made using the student's *t*-test. Differences among the means were considered to be statistically significant at a *P*-value of <0.05 and <0.01.

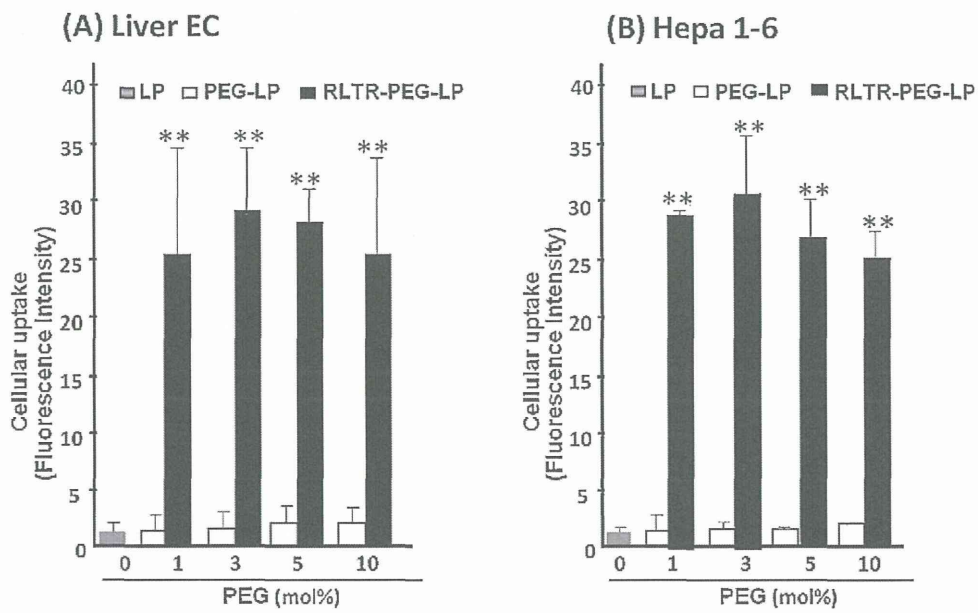

Fig. 1. Cellular uptake of RLTR-PEG-LPs. For the cellular uptake study, 40,000 cells/well were seeded in a 24-well plate. After 24 h LPs modified with different mol% of PEG-DSPE or RLTR-PEG-DSPE were incubated with (A) liver EC or (B) Hepa1-6 cells for 3 h and the cellular uptake efficiency of the prepared rhodamine labeled LPs were determined by measuring the fluorescence intensity of rhodamine. Cellular uptake is expressed as the mean ± SD ($n = 3$) and statistical analysis vs. LP was performed by One-way ANOVA followed by Dunnett-test. **$P < 0.01$.

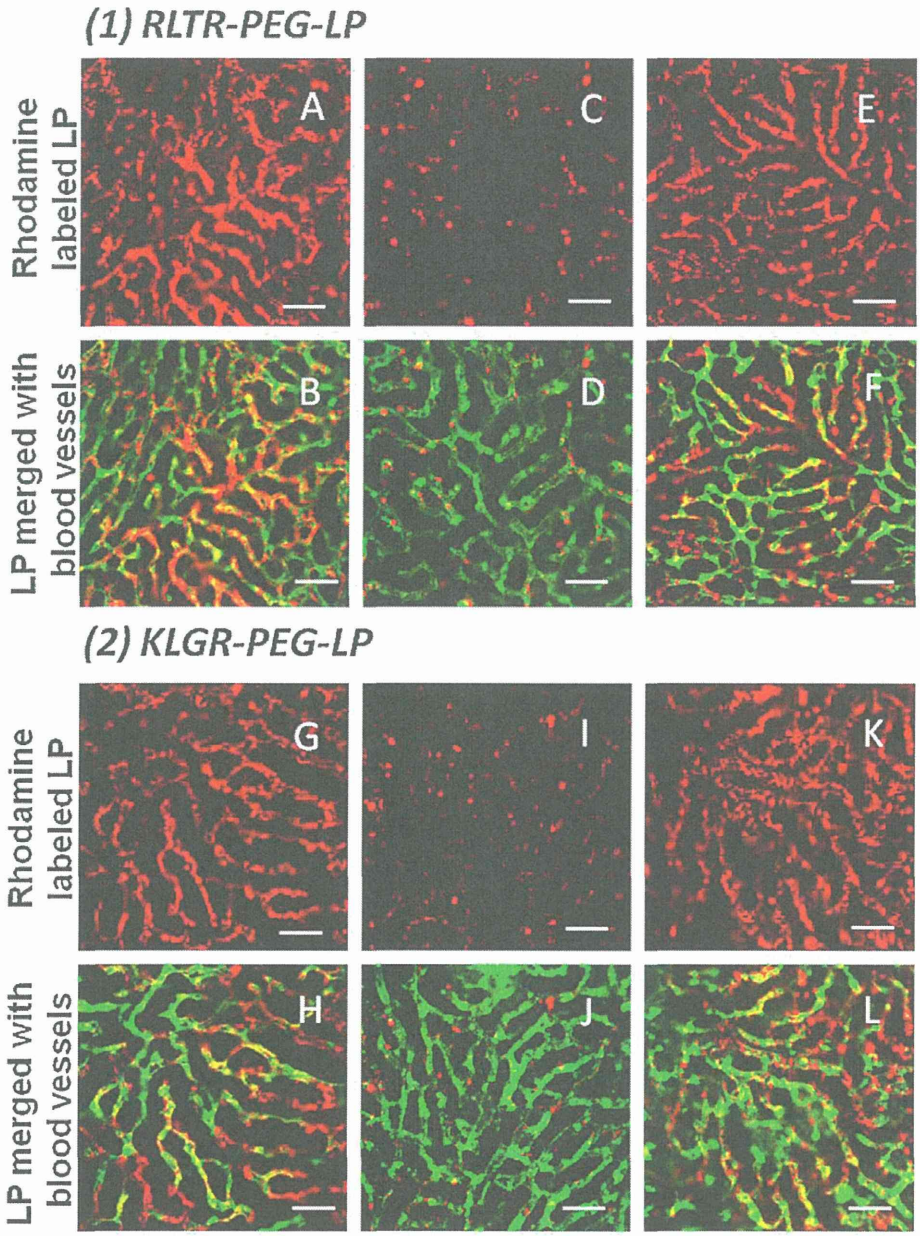

Fig. 4. In vivo competitive inhibition studies of RLTR-PEG-LPs or KLGR-PEG-LPs using unlabeled RLTR-PEG-LPs or KLGR-PEG-LPs or cationic LPs. Green and red color represents blood vessels stained by Isolectin B4 and rhodamine labeled LPs respectively. Mice were pretreated with unlabeled RLTR-PEG-LPs or KLGR-PEG-LPs or cationic LPs 15 min before the second treatment with labeled RLTR-PEG-LPs or KLGR-PEG-LPs for another 25 min of incubation. Representative images of liver tissues with (A and B) labeled RLTR-PEG-LPs, (C and D) labeled RLTR-PEG-LPs pre-treated with unlabeled RLTR-PEG-LPs, (E and F) labeled RLTR-PEG-LPs pre-treated with unlabeled cationic LPs, (G and H) labeled KLGR-PEG-LPs, (I and J) labeled KLGR-PEG-LPs pre-treated with unlabeled KLGR-PEG-LPs, (K and L) labeled KLGR-PEG-LPs pre-treated with unlabeled cationic LPs are shown. Scale bars correspond to 50 μm in all images.

LPs was quite different from that of the RLTR-PEG-LPs, in which the cationic LPs were gathered in particular spots (Fig. 3D). In addition, these dots did not overlap with liver endothelial cells (Fig. 3E and F) indicating that they were taken up by non-parenchymal cells such as Kupffer cells or were merely aggregated LPs.

3.4. In vivo inhibition study

In order to examine some possible mechanisms of unique targeting ability of RLTR peptide into liver endothelial cells, comparative studies of RLTR and its reversed peptide sequence named as KLGR were performed in the following part. Both RLTR-PEG-LPs and KLGR-PEG-LPs were accumulated along with the liver blood vessels (Fig. 4A and B, G and H). Next, accumulation of both labeled RLTR-PEG-LPs and KLGR-PEG-LP along with the liver blood vessels were dramatically inhibited by a pre-treatment with unlabeled RLTR-PEG-LPs or KLGR-PEG-LPs (Fig. 4C and D, I and J), however, small portions of signal were remaining. In contrast, the accumulation of both labeled RLTR-PEG-LPs or KLGR-PEG-LP was not reduced by the pre-treatment with unlabeled cationic LPs (Fig. 4E and F, K and L). The results generated in this study suggest that cationic charge is not the reason for this uptake and may be both RLTR peptide and its reverse sequence, the KLGR peptide has some specificity for liver endothelial cells. Possible interpretations will be discussed in Section 4.

3.5. In vitro comparative inhibition study of RLTR-PEG-LPs

This experiment was performed to support the in vivo inhibition data. We compared the cellular uptake of both RLTR-PEG-LPs and

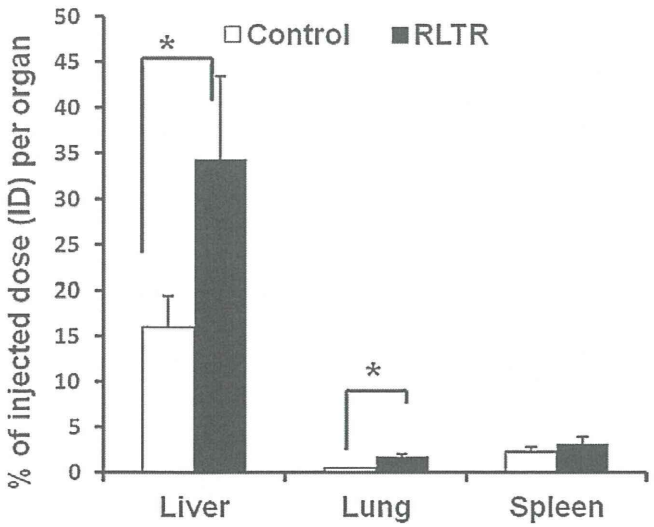

Fig. 2. Biodistribution of ^{3}H-CHE labeled RLTR-PEG-LPs and LPs in different organ. Male ICR mice were intravenously injected with labeled RLTR-PEG-LPs and LPs. After 25 min of incubation different organs of mouse were collected and radioactivity was measured. Tissue accumulation of LPs was represented as % of injected dose (ID). Here, % of ID is expressed as the mean ± SD (n = 4). Statistical analyses were performed by the unpaired Student's t-test, where *P < 0.05.

3. Results

3.1. Synthesis of RLTR-PEG-DSPE

The thiol group of the cystein residue in the RLTR peptide was conjugated by reaction with Mal-PEG$_{2000}$-DSPE at 37 °C for 24 h (Reaction scheme is shown in the supplementary figure 1). MALDI-TOF MS analyses confirmed the synthesis of RLTR-PEG-DSPE.

Supplementary material related to this article can be found, in the online version, at http://dx.doi.org/10.1016/j.ijpharm.2013.07.068.

3.2. The characteristic of RLTR-PEG-LPs and its cellular uptake

The selected RLTR peptide was attached to the top of PEG in PEGylated liposomes. PEG liposomes (PEG-LPs) and RLTR modified PEG liposomes (RLTR-PEG-LPs) were prepared by incorporating PEG-DSPE or RLTR-PEG-DSPE at levels of 1, 3, 5, or 10 mol% of the total lipid. The physical properties of the prepared LPs are shown in Table 1. To evaluate the effect of the RLTR peptide on cellular uptake, we next examined the cellular uptake of RLTR-PEG-LPs and PEG-LPs in primary liver endothelial cells (LECs) and in Hepa1-6 cell line. The RLTR peptide enhanced the cellular uptake of PEG-LPs and the maximum cellular uptake was observed within 3 mol% of RLTR peptide modification in both the cells (Fig. 1A and B).

3.3. In vivo selectivity of RLTR peptide

A biodistribution study of RLTR-PEG-LPs was carried out in order to confirm the targeting ability of RLTR-PEG modified LP. Compared to unmodified control LPs, RLTR-PEG-LPs were largely accumulated in the liver, with only negligible accumulation in the lung or spleen, within a very short time (Fig. 2). The liver targeting ability of RLTR peptide was more than its ability to target lung or spleen. We then obtained an in vivo image of the liver to check the distribution pattern of this RLTR-PEG modified LP in liver.

We then performed an in vivo accumulation study to verify our hypothesis outlined in the introduction part. We investigated the intrahepatic distribution of RLTR-PEG-LPs by confocal microscopy. Rhodamine-labeled RLTR-PEG-LPs were widely distributed throughout the blood vessels (Fig. 3A), and these intensities were essentially merged with the signal for Isolectin B4, a marker of endothelial cells (Fig. 3B and C). These results demonstrate that RLTR-PEG-LPs efficiently target liver endothelial cells rather than hepatocytes. Furthermore, we compared the intrahepatic distribution pattern with RLTR-PEG-LPs and cationic LPs in order to evaluate the effect of the cationic charge of the liposomal surface. The size and zeta-potential of the rhodamine-labeled RLTR-PEG-LPs and cationic LPs was 125 nm, 26 mV and 132 nm, 22 mV respectively. The intrahepatic distribution pattern of the cationic

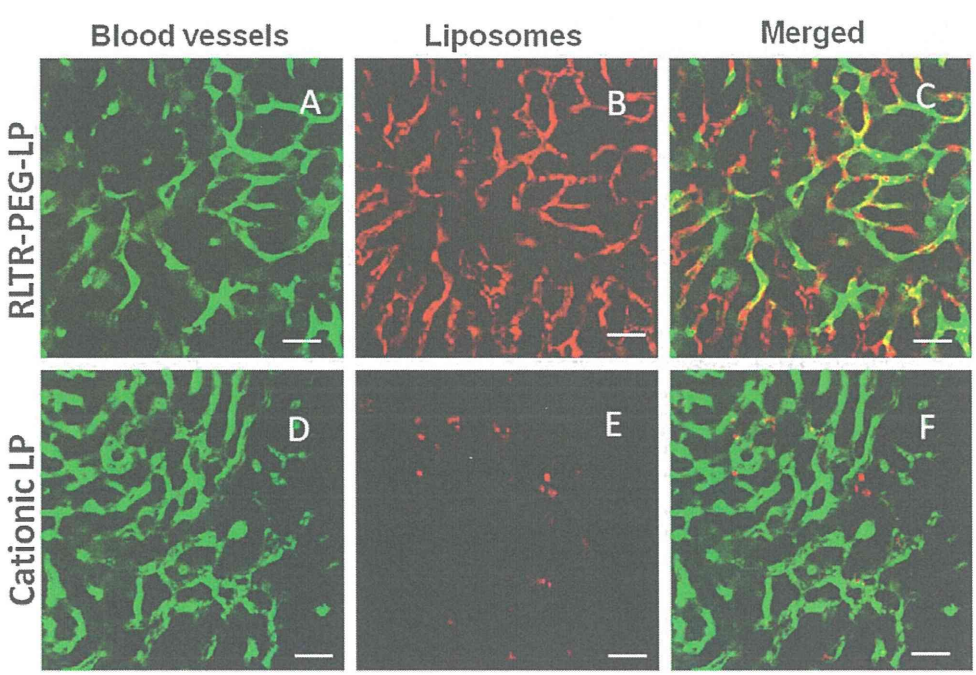

Fig. 3. Representative intrahepatic distribution pattern of RLTR-PEG-LPs (A–C) and a cationic control LPs, in which the lipid composition was DC6-14/DOPE/Chol = 4:3:3 (D–F). Green and red color represents blood vessels stained by Isolectin B4 and rhodamine labeled LPs respectively. Scale bars correspond to 50 μm in all images.